Structural Properties of the Cr(III)−Fe(III) (Oxy)hydroxide Compositional Series: Insights for a Nanomaterial "Solid Solution"

Yuanzhi Tang,*[†,‡] F. Marc Michel,[†,‡,⊥] Lihua Zhang,[§] Richard Harrington,[†,||] John B. Parise,[†,‡,||] and Richard J. Reeder[†,‡]

[†]*Department of Geosciences, Stony Brook University, Stony Brook, New York 11794-2100,* [‡]*Center for Environmental Molecular Science, Stony Brook University, Stony Brook, New York 11794-2100,* [§]*Center for Functional Nanomaterials, Brookhaven National Laboratory, Upton, New York 11973, and* [||]*Department of Chemistry, Stony Brook University, Stony Brook, New York 11794-3400.* [⊥]*Present address: Department of Geological and Environmental Sciences, Stanford University, Stanford, CA 94305.*

Chromium(III) (oxy)hydroxide and mixed Cr(III)−Fe(III) (oxy)hydroxides are environmentally important compounds for controlling chromium speciation and bioaccessibility in soils and aquatic systems and are also industrially important as precursors for materials and catalyst synthesis. However, direct characterization of the atomic arrangements of these materials is complicated because of their amorphous X-ray properties. This study involves synthesis of the complete Cr(III)−Fe(III) (oxy)hydroxide compositional series, and the use of complementary thermal, microscopic, spectroscopic, and scattering techniques for the evaluation of their structural properties. Thermal analysis results show that the Cr end member has a higher hydration state than the Fe end member, likely associated with the difference in water exchange rates in the first hydration spheres of Cr(III) and Fe(III). Three stages of weight loss are observed and are likely related to the loss of surface/structural water and hydroxyl groups. As compared to the Cr end member, the intermediate composition sample shows lower dehydration temperatures and a higher exothermic transition temperature. XANES analysis shows Cr(III) and Fe(III) to be the dominant oxidation states. XANES spectra also show progressive changes in the local structure around Cr and Fe atoms over the series. Pair distribution function (PDF) analysis of synchrotron X-ray total scattering data shows that the Fe end member is nanocrystalline ferrihydrite with an intermediate-range order and average coherent domain size of ∼27 Å. The Cr end member, with a coherent domain size of ∼10 Å, has only short-range order. The PDFs show progressive structural changes across the compositional series. High-resolution transmission electron microscopy (HRTEM) results also show the loss of structural order with increasing Cr content. These observations provide strong structural evidence of chemical substitution and progressive structural changes along the compositional series.

1. Introduction

Chromium is one of the most significant anthropogenic metal contaminants. Its presence in soils and aquatic systems results from its widespread industrial applications, such as tanning, metallurgy, plating, and use as an anticorrosion agent. The toxicity and transport behavior of Cr depend strongly on its valence. The most common oxidation states in the environment are hexavalent and trivalent. Cr(VI) exists primarily in the form of bichromate ($HCrO_4^-$) and chromate (CrO_4^{2-}), which are strong oxidants and considered carcinogenic with inhalation exposure.[1] Cr(VI) compounds are typically soluble in natural water and, thus, mobile and bioaccessible. Cr(III)

usually forms insoluble oxides and (oxy)hydroxides and, except in large amounts, is considered an essential nutrient rather than a health risk.[1]

Interaction of chromium with minerals can greatly affect its chemical speciation and therefore its mobility in soil and aquatic systems. Interactions with iron-containing minerals, which are common in surface environments, are especially important because of the potential for redox reactions. Reduction of Cr(VI) to Cr(III) by iron-containing reductants, such as zero-valent Fe and Fe(II)-bearing minerals, has been considered for

---

*To whom correspondence should be addressed. Present address: School of Engineering and Applied Sciences, Harvard University, 58 Oxford St., ESL, Cambridge, MA 02138. Phone: (617) 496-3559. Fax: (617) 496-1023. E-mail: ytang@seas.harvard.edu.

(1) Beliles, R. P. The Lesser Metals. In *Toxicity of Heavy Metals in the Environment* (*Part II*); Oehme, F. W., Ed.; Marcel Dekker: New York, 1979.

(2) U.S. Environmental Protection Agency (EPA). Control and treatment technology for the metal finishing industry. Sulfide precipitation; EPA Technical Report 625/8-80-003; U.S. Government Printing Office: Washington, DC, 1980.

(3) Blowes, D. W.; Ptacek, C. J.; Jambor, J. L. *Environ. Sci. Technol.* **1997**, *31*(12), 3348–3357.

(4) Patterson, R. R.; Fendorf, S.; Fendorf, M. *Environ. Sci. Technol.* **1997**, *31*(7), 2039–2044.

(5) Loyaux-Lawniczak, S.; Refait, P.; Ehrhardt, J. J.; Lecomte, P.; Genin, J. M. R. *Environ. Sci. Technol.* **2000**, *34*(3), 438–443.

remediation of Cr(VI)-containing waste waters.[2−7] The resulting Cr(III) (oxy)hydroxide and/or Cr(III)−Fe(III) (oxy)hydroxide phases [hereafter termed Cr-(oxy)hydroxide and $Cr_xFe_{1−x}$-(oxy)hydroxide, respectively] have very low solubilities,[8,9] allowing effective sequestration of Cr at contaminated sites. Experiments have shown that the solubility of $Cr_xFe_{1−x}$-(oxy)hydroxide intermediate compositions is lower than that of the Cr-(oxy)hydroxide end member composition.[8] Cr-(oxy)hydroxide or Cr_x-$Fe_{1−x}$-(oxy)hydroxide phases can also form via coprecipitation of Cr(III) and Fe(III) at neutral to alkaline pH[8] or as a sorption/surface precipitation product during sorption of Cr(III) onto ferrihydrite or other minerals.[10,11] Because of their low solubility, these phases may control the fate of Cr(III) in contaminated soils and other impacted environments such as acid mine drainage sites.[12]

Cr-(oxy)hydroxide phases have been the focus of much study because of their role in the production of Cr(III) oxide catalysts and the wide variety of their uses in other applications, such as green pigments and coating materials for thermal protection and wear resistance.[13−15] Thermal and chemical transformations of Cr-(oxy)hydroxide have been extensively studied for synthesis of Cr_2O_3.[16−18] Coprecipitated $Cr_xFe_{1−x}$-(oxy)hydroxide has also been proposed for making $Cr_2O_3−Fe_2O_3$-based oxide mixtures for reference electrodes for oxygen sensors.[19]

Despite the widespread interest in $Cr_xFe_{1−x}$-(oxy)hydroxide phases, uncertainties concerning their stoichiometry and structure remain. The Cr end member, Cr-(oxy)hydroxide, is variously termed chromium hydroxide, $Cr(OH)_3$, $Cr(OH)_3 \cdot nH_2O$, hydrate chromium oxide/chromium hydrous oxide, or chromia gel. It exhibits broad, diffuse features in X-ray diffraction patterns that are typical of poorly crystalline or amorphous materials. Extensive studies have addressed the hydrolysis, precipitation, and oligomerization of Cr(III) under aqueous conditions,[20−26] the preparation and thermal evolution of Cr-(oxy)hydroxide,[14,16,27,28] its solubility and oxidation behavior under different conditions,[8,9,29−31] and its structural properties, which vary with experimental conditions.[11,14,16,31−33]

A complete series of mixed composition $Cr_xFe_{1−x}$-(oxy)hydroxide compounds can be synthesized between the pure Cr and Fe end members, which, together with solubility and FT-IR evidence, suggests that the series may represent a continuous solid solution.[8,21,34] However, characterization of this series is incomplete. The lack of direct structural characterization of the Cr end member as well as of mixed composition solids limits our understanding of the environmental and materials properties of these phases, as well as their reactivities in aqueous solutions. In this study, we use complementary techniques to examine the structural properties of the mixed composition solids. Thermogravimetric−differential scanning calorimetry (TG-DSC) analysis, X-ray diffraction (XRD), high-resolution transmission electron microscopy (HRTEM), pair distribution function (PDF) analysis of synchrotron X-ray total scattering data, and both Cr and Fe K-edge X-ray absorption spectroscopy (XAS) provide new insights into the following fundamental questions: (1) What is the degree of structural order (i.e., short-, intermediate-, or long-range order) of the $Cr_xFe_{1−x}$-(oxy)hydroxide samples. (2) Do they represent a physical mixture of distinct phases, or are they single phase with chemical substitution? If it is the latter, (3) do they form a continuous solid solution? Finally, we provide some constraints that can be used for a more complete characterization of the structure changes across the compositional series. The results provide valuable information relevant to understanding the natural speciation of Cr and remediation methods based on the reduction of Cr(VI) to Cr(III), contributing to a structural basis for materials processing using $Cr_xFe_{1−x}$-(oxy)hydroxide as a precursor.

(6) Hansel, C. M.; Wielinga, B. W.; Fendorf, S. R. *Geochim. Cosmochim. Acta* **2003**, *67*(3), 401–412.
(7) Manning, B. A.; Kiser, J. R.; Kwon, H.; Kanel, S. R. *Environ. Sci. Technol.* **2007**, *41*(2), 586–592.
(8) Sass, B. M.; Rai, D. *Inorg. Chem.* **1987**, *26*(14), 2228–2232.
(9) Ziemniak, S. E.; Jones, M. E.; Combs, K. E. S. *J. Solution Chem.* **1998**, *27*(1), 33–66.
(10) Fendorf, S. E.; Lamble, G. M.; Stapleton, M. G.; Kelley, M. J.; Sparks, D. L. *Environ. Sci. Technol.* **1994**, *28*(2), 284–289.
(11) Charlet, L.; Manceau, A. *J. Colloid Interface Sci.* **1992**, *148*(2), 443–458.
(12) Doelsch, E.; Basile-Doelsch, I.; Rose, J.; Masion, A.; Borschneck, D.; Hazemann, J. L.; Saint Macary, H.; Borrero, J. Y. *Environ. Sci. Technol.* **2006**, *40*(24), 7602–7608.
(13) Busca, G.; Ramis, G.; Prieto, M. D.; Escribano, V. S. *J. Mater. Chem.* **1993**, *3*(6), 665–673.
(14) Abecassis-Wolfovich, M.; Rotter, H.; Landau, M. V.; Korin, E.; Erenburg, A. I.; Mogilyansky, D.; Gartstein, E. *J. Non-Cryst. Solids* **2003**, *318*(1−2), 95–111.
(15) Xu, H. T.; Lou, T. J.; Li, Y. D. *Inorg. Chem. Commun.* **2004**, *7*(5), 666–668.
(16) Ratnasamy, P.; Leonard, A. J. *J. Phys. Chem.* **1972**, *76*(13), 1838–1843.
(17) Onjia, A. E.; Milonjic, S. K.; Cokesa, D.; Comor, M.; Miljevic, N. *Mater. Res. Bull.* **2003**, *38*(8), 1329–1339.
(18) Yao, Z. M.; Li, Z. H.; Zhang, Y. *J. Colloid Interface Sci.* **2003**, *266*(2), 382–387.
(19) Soykan, H. S.; Karakas, Y. *Powder Metall.* **2007**, *50*(1), 72–75.
(20) Spiccia, L.; Marty, W. *Inorg. Chem.* **1986**, *25*(3), 266–271.
(21) Rai, D.; Sass, B. M.; Moore, D. A. *Inorg. Chem.* **1987**, *26*(3), 345–349.
(22) Livage, J.; Henry, M.; Sanchez, C. *Prog. Solid State Chem.* **1988**, *18*(4), 259–341.
(23) Spiccia, L.; Marty, W.; Giovanoli, R. *Inorg. Chem.* **1988**, *27*(15), 2660–2666.
(24) Rao, L. F.; Zhang, Z. C.; Friese, J. I.; Ritherdon, B.; Clark, S. B.; Hess, N. J.; Rai, D. *J. Chem. Soc., Dalton Trans.* **2002**, No. 2, 267–274.
(25) Rustad, J. R.; Casey, W. H. *J. Phys. Chem. B* **2006**, *110*(14), 7107–7112.
(26) Spiccia, L.; Casey, W. H. *Geochim. Cosmochim. Acta* **2007**, *71*(23), 5590–5604.
(27) Music, S.; Maljkovic, M.; Popovic, S.; Trojko, R. *Croat. Chem. Acta* **1999**, *72*(4), 789–802.
(28) Gash, A. E.; Tillotson, T. M.; Satcher, J. H.; Hrubesh, L. W.; Simpson, R. L. *J. Non-Cryst. Solids* **2001**, *285*(1−3), 22–28.
(29) Rai, D.; Hess, N. J.; Rao, L. F.; Zhang, Z. C.; Felmy, A. R.; Moore, D. A.; Clark, S. B.; Lumetta, G. J. *J. Solution Chem.* **2002**, *31*(5), 343–367.
(30) Lee, G. H.; Hering, J. G. *Environ. Sci. Technol.* **2005**, *39*(13), 4921–4928.
(31) Rai, D.; Moore, D. A.; Hess, N. J.; Rosso, K. M.; Rao, L.; Heald, S. M. *J. Solution Chem.* **2007**, *36*(10), 1261–1285.
(32) Manceau, A.; Charlet, L. *J. Colloid Interface Sci.* **1992**, *148*(2), 425–442.
(33) Kucheyev, S. O.; Sadigh, B.; Baumann, T. F.; Wang, Y. M.; Felter, T. E.; van Buuren, T.; Gash, A. E.; Satcher, J. H.; Hamza, A. V. *J. Appl. Phys.* **2007**, *101*(12), 124315 .
(34) Amonette, J. E.; Rai, D. *Clays Clay Miner.* **1990**, *38*(2), 129–136.

Table 1. Information about Sample Composition and Parameters for PDF Analysis[a]

	ratio in solution		ratio in final solid		approximate formula used for PDF normalization[b]	coherent domain size (Å)[c]
sample	Fe	Cr	Fe	Cr		
Fe10	1	–	1	–	$Fe_2O_3 \cdot 2.5H_2O$	27
Fe9Cr1	0.9	0.1	0.92	0.08	$(Cr_{0.08}Fe_{0.92})_2O_3 \cdot 3.3H_2O$	25
Fe8Cr2	0.8	0.2	0.84	0.16	$(Cr_{0.16}Fe_{0.84})_2O_3 \cdot 4.1H_2O$	22
Fe7Cr3	0.7	0.3	0.72	0.28	$(Cr_{0.28}Fe_{0.72})_2O_3 \cdot 4.9H_2O$	19
Fe6Cr4	0.6	0.4	0.67	0.33	$(Cr_{0.33}Fe_{0.67})_2O_3 \cdot 5.6H_2O$	18
Fe5Cr5	0.5	0.5	0.57	0.43	$(Cr_{0.43}Fe_{0.57})_2O_3 \cdot 8.8H_2O$	14
Fe4Cr6	0.4	0.6	0.47	0.52		
Fe3Cr7	0.3	0.7	0.36	0.64	$(Cr_{0.64}Fe_{0.36})_2O_3 \cdot 9.8H_2O$	13
Fe2Cr8	0.2	0.8	0.23	0.77	$(Cr_{0.77}Fe_{0.23})_2O_3 \cdot 10H_2O$	12
Fe1Cr9	0.1	0.9	0.13	0.87		
Cr10	–	1	–	1	$Cr_2O_3 \cdot 10H_2O$	10

[a] The maximum Q range used for PDF analysis is 29 Å^{-1} for all samples. [b] Estimated from composition (DCP) and thermal analysis (TG). [c] Estimated from attenuation of correlations in PDF.

2. Experimental Section

2.1. Synthesis of Cr$_x$Fe$_{1-x}$-(oxy)hydroxides. Many different synthesis methods have been used to produce the Cr$_x$Fe$_{1-x}$-(oxy)hydroxide, most commonly by reduction of Cr(VI) by Fe(II)-containing compounds or by hydrolysis of Cr(III)- and Fe(III)-containing solutions using different alkaline sources. To produce the whole compositional series, we adapted the synthesis method of Hansel et al.,[6] which is representative of commonly occurring environmental conditions. Fe(NO$_3$)$_3$·9H$_2$O and Cr(NO$_3$)$_3$·9H$_2$O (both from Alfa Aesar) were dissolved in 80 mL of deionized water to produce a total metal concentration of 0.1 M with desired Cr(III):Fe(III) molar ratios. The solutions were slowly titrated to pH 7 with 1 M NaOH. Precipitates formed from the suspension were aged for 24 h before being repeatedly centrifuged, decanted, and rinsed with deionized water to remove the remaining electrolytes. The resulting wet pastes were recovered and dried in an oven at 60 °C. The dry powders or cakes obtained were gently ground. The color of the powders differed progressively according to their compositions, from reddish brown for the Fe end member to olive green for the Cr end member. Samples were labeled according to the starting Fe:Cr molar ratios (Table 1); e.g., Fe10 is the pure Fe end member, whereas Fe6Cr4 is the Cr$_x$Fe$_{1-x}$-(oxy)hydroxide with an initial x value of 0.4 and a 60:40 Fe:Cr molar ratio. Portions of the powders were dissolved in a mixture of hydrochloric acid and nitric acid for analysis of Cr and Fe composition by direct current plasma (DCP) spectrometry. Details of the structural characterization by XRD, TG-DSC, HRTEM, PDF, and XAS are given later.

2.2. Model Compounds. Several Fe(III)- or Cr(III)-containing compounds were used for PDF and XAS comparison with Cr$_x$Fe$_{1-x}$-(oxy)hydroxide samples: 2-line ferrihydrite (provided by D. Hausner, Temple University, Philadelphia, PA), goethite, Cr$_2$O$_3$ (Acros Organics), and 0.1 M K$_2$CrO$_4$ (Acros Organics) aqueous solution. The K$_2$CrO$_4$ aqueous solution has a pH value of 12. Speciation calculation using Phreeqc[35] shows that essentially 100% of the Cr(VI) is a CrO$_4^{2-}$ species, with Cr in tetrahedral coordination. The 2-line ferrihydrite was synthesized using the method developed by Schwertmann and

Cornell.[36] A 1 M solution of NaOH (Sigma-Aldrich) was added at a rate of 2 mL/min to a 0.2 M solution of Fe(NO$_3$) (Sigma-Aldrich) with constant stirring until the pH reached 7.5. The solution was repeatedly washed with deionized water and centrifuged to remove the remaining electrolytes, followed by natural drying in a hood. Goethite was synthesized following the method of Sileo et al.[37] and Schwertmann and Cornell;[36] 100 mL of a 1 M Fe(NO$_3$)$_3$ solution was added to 180 mL of a 5 M KOH solution. The obtained suspension was diluted to 2 L with deionized water and aged for 60 h at 70 °C in a closed polypropylene bottle. The solid was recovered by repeated filtration and washing with deionized water and drying at 60 °C and was ground for structural analysis. X-ray diffraction confirmed its structure to be goethite.

2.3. X-ray Diffraction Analysis. High-energy X-ray total scattering data of the Cr$_x$Fe$_{1-x}$-(oxy)hydroxide compositional series were collected at beamline 1-ID-C[38] [~100 keV, λ = 0.1240(6) Å] of the Advanced Photon Source, Argonne National Laboratory (APS-ANL, Argonne, IL). An amorphous Si area detector system manufactured by General Electric was used for data collection. A CeO$_2$ standard (NIST diffraction intensity standard set 674a) was used to calibrate the sample-to-detector distance and the nonorthogonality of the detector relative to the incident beam. Conversion of data from two dimensions to one dimension was performed using Fit2D.[39,40]

The experimental total scattering structure function $S(Q)$, reduced experimental structure function $f(Q)$, and PDF, or $G(r)$, were obtained using PDFgetX2.[41] Compositions used for the normalization of the experimental structure functions are included in Table 1. Since we currently do not have detailed structure models for the compositional series, it is difficult to estimate the exact chemical formulas of each sample, which would provide the most favorable basis for normalization. Therefore, we adopted a self-consistent method, assuming the general formula of (Cr,Fe)$_2$O$_3$·nH$_2$O for all samples. We note that a choice of a different general formula could also be used, as long as the normalization approach is consistent. Information obtained regarding the Fe:Cr ratio (from DCP analysis) was

(35) Parkhurst, D. L.; Appelo, C. A. J. User's guide to PHREEQC (Version 2): A computer program for speciation, batch-reaction, one-dimensional transport, and inverse geochemical calculations. Water Research Investigative Report 99-4259; U.S. Geological Survey: 1999; p 310.

(36) Schwertmann, U.; Cornell, R. M. *Iron Oxides in the Laboratory: Preparation and Characterization*, 1st ed.; Wiley-VCH: Weinheim, Germany, 2000.

(37) Sileo, E. E.; Ramos, A. Y.; Magaz, G. E.; Blesa, M. A. *Geochim. Cosmochim. Acta* **2004**, *68*(14), 3053–3063.

(38) Shastri, S. D.; Fezzaa, K.; Mashayekhi, A.; Lee, W. K.; Fernandez, P. B.; Lee, P. L. *J. Synchrotron Radiat.* **2002**, *9*, 317–322.

(39) Hammersley, A. P.; Svensson, S. O.; Hanfland, M.; Fitch, A. N.; Hausermann, D. *High Pressure Res.* **1996**, *14*, 235–248.

(40) Hammersley, A. P. Fit2D Version 9.129 Reference Manual version 3.1; ESRF98HA01T; ESRF Internal Report: **1998**.

(41) Qiu, X.; Thompson, J. W.; Billenge, S. J. L. *J. Appl. Crystallogr.* **2004**, *37*, 678.

incorporated in the compositions used for PDF normalization. Vajpei et al.[42] studied the thermal behavior of coprecipitated Fe(III)−Cr(III) hydroxide series with a synthesis method similar to ours and found gradual changes in weight loss due to hydration within the series. Assuming that the total weight loss is due to the removal of surface or structural water, total hydration information (from TG weight loss analysis) of the Fe end member (Fe10), Cr end member (Cr10), and intermediate composition sample (Fe5Cr5) is used for these three samples as well as for estimating the hydration states of all other samples. This hydration information is also incorporated in the normalization. Details of the approximate formulas used for PDF normalization are listed in Table 1. This normalization approach resulted in consistent reduced structure functions for all samples, and the PDFs were calculated from the Fourier transforms of these data truncated at 29 Å^{-1}. The size of the coherent scattering domain for each sample was estimated from the attenuation of the PDF as a function of r (angstroms) and falls within the instrument envelope for beamline 1-ID-C.[43]

2.4. Thermal Analysis. Thermal gravimetric (TG) and differential scanning calorimetry (DSC) analyses of the Cr_xFe_{1-x}-(oxy)hydroxide samples were conducted using a Netzsch STA 449C Jupiter instrument with flowing dry air over the range of 25−800 °C and a heating rate of 10 °C/min.

2.5. High-Resolution Transmission Electron Microscopy Characterization. High-resolution transmission electron microscopy (HRTEM) images of the Cr_xFe_{1-x}-(oxy)hydroxide samples were recorded on a JEOL 2100F instrument, operating at 200 keV, at the Center for Functional Nanomaterials (CFN) at Brookhaven National Laboratory (BNL). A small amount of each sample was dispersed in deionized water and ultrasonicated for ∼1 min. Then a drop of the suspension was placed onto a 300-mesh Cu grid with a lacey-carbon support film and air-dried. To avoid beam damage, image focus was obtained on the carbon film adjacent to the particles of interest, and then the beam was moved onto the sample particle. Because of the small particle sizes (1−2 nm) and strong aggregation of these samples, selected area electron diffraction (SAED) patterns and energy dispersive spectra (EDS) were obtained from areas of large aggregates (> 50 nm).

2.6. X-ray Absorption Near-Edge Structure (XANES) Spectroscopy. Cr and Fe K-edge XANES spectra were collected for samples spanning the whole Cr_xFe_{1-x}-(oxy)hydroxide series and for selected model compounds at the bending-magnet beamline at sector 12 (operated by BESSRC-CAT) of the APS-ANL and beamline X11B of the National Synchrotron Light Source (NSLS) at BNL. Depending on Cr or Fe concentrations, data on the Cr_xFe_{1-x}-(oxy)hydroxide samples were collected in either (1) transmission mode, with sample powders brushed on several layers of Kapton tape or mixed with BN in a Lucite sample holder and placed at 90° to the incident beam, or (2) fluorescence mode, with samples brushed on Kapton tape, positioned at 45° to the incident beam, using a Lytle detector positioned 90° to the incident beam. Data for the Cr- or Fe-containing model compounds were collected in transmission mode. Energy calibration used Cr or Fe metal foils. For both beamlines, a pair of Si(111) crystals was used for the monochromator, with one crystal detuned by 40% for both Cr and Fe K-edges to minimize third-order harmonics. Data processing was performed with the data analysis program WinXAS.[44]
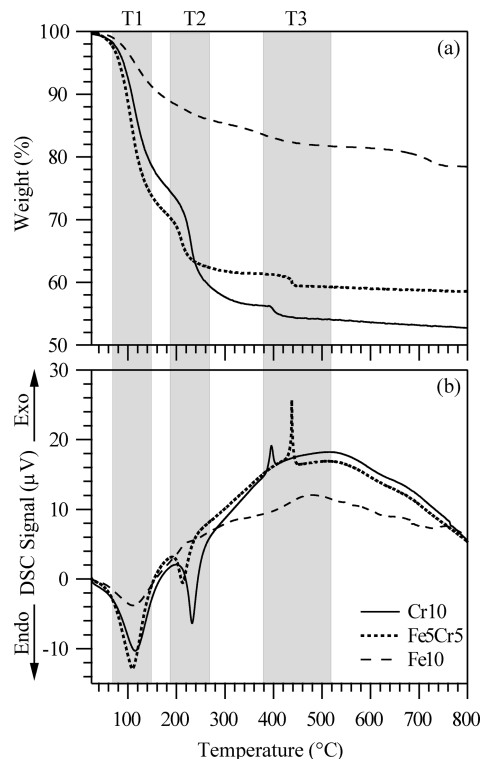

Figure 1. (a) Thermogravimetric (TG) and (b) differential scanning calorimetry (DSC) data for Cr10, Fe5Cr5, and Fe10. Shaded areas shows the three stages of weight loss, labeled as T1, T2, and T3.

3. Results

3.1. Composition and Thermal Analysis. Eleven samples in the Cr_xFe_{1-x}-(oxy)hydroxide series were synthesized with x from 0 to 1. Fe:Cr molar ratios in the starting solution and final solids (as analyzed by DCP) are listed in Table 1.

Thermal analysis (TG-DSC) results for Cr10, Fe5Cr5, and Fe10 are shown in Figure 1. Cr10 shows three stages of weight loss, with a total weight loss of ∼47% at ∼800 °C. The first stage (T1) shows a gradual weight loss, with a corresponding broad endothermic DSC peak centered at ∼100 °C. Weight loss at this low temperature is normally attributable to the loss of loosely bound or surface-adsorbed water. The second stage, T2, occurs over a narrow temperature interval, 200−250 °C, with a corresponding sharp endothermic DSC peak at ∼230 °C, possibly due to the loss of structural water. These two stages contribute the greatest fraction of weight loss in Cr10, suggesting a large degree of hydrolysis. Weight loss during the third stage (T3) is small by comparison and occurs over a narrow temperature range (∼400 °C), accompanied by a sharp exothermic DSC peak at ∼400 °C. This stage is associated with the sample glowing as a result of rapid oxidation and reduction between Cr(III) and higher oxidation states, and subsequent formation of nanocrystalline Cr_2O_3.[14,45,46]

(42) Vajpei, A. C.; Rousset, A.; Uma; Chandra, K.; Saraswat, I. P.; Mathur, V. K. *Solid State Ionics* **1989**, *32−33*, 741–748.
(43) Michel, F. M.; Schoonen, M. A. A.; Zhang, X. V.; Martin, S. T.; Parise, J. B. *Chem. Mater.* **2006**, *18*(7), 1726–1736.
(44) Ressler, T. *J. Phys. IV* **1997**, *7*, 269–270.
(45) Fahim, R. B.; Gabr, R. M.; Zaki, M. I.; Mansour, S. A. A. *J. Colloid Interface Sci.* **1981**, *81*(2), 468–476.
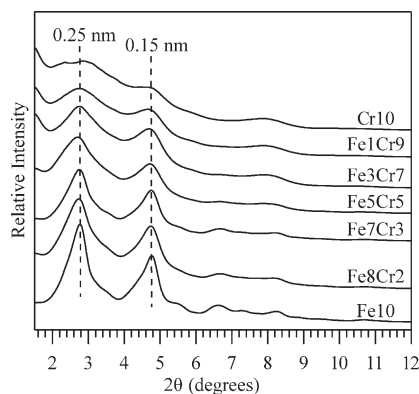(46) Carruthe, J. D.; Sing, K. S. W. *Nature* **1967**, *213*(5071), 66–68.

Article

Chem. Mater., Vol. 22, No. 12, 2010 3593

Figure 2. X-ray diffractograms of samples spanning the Cr_xFe_{1-x}-(oxy)hydroxide series ($\lambda = 0.1240(6)$ Å).

Figure 3. (a) Cr K-edge XANES spectra of Cr_xFe_{1-x}-(oxy)hydroxide samples and the model compounds Cr_2O_3 and CrO_4^{2-} (aq). The sharp feature at ~5980 eV indicated by the asterisk is a monochromator glitch. (b) Corresponding first derivatives. Vertical dashed lines indicate points at which progressive changes are observed.

The Fe end member, Fe10, shows a smaller, more gradual weight loss (~22%) than Cr10 does. It also shows the endothermic peak at ~110 °C, corresponding to the loss of surface-adsorbed water, but no endothermic peak as observed for Cr10 at ~230 °C. Fe10 shows a broad exothermic peak at ~480 °C, in contrast to the sharp exothermic peak observed for Cr10 at a lower temperature (~400 °C).

Interestingly, the intermediate phase Fe5Cr5 also shows three stages of weight loss, totaling ~42% at 800 °C, with dehydration stages T1 and T2 shifted to lower temperatures. It also shows a strong exothermic peak at ~440 °C (T3), which is stronger in intensity and shifted to a higher temperature compared to that of Cr10 (at ~400 °C).

3.2. Bulk X-ray Diffraction Characteristics. Initial inspection of all samples was performed using the low-2θ region of synchrotron X-ray diffraction patterns (Figure 2, with increasing Cr contents from bottom to the top). Fe end member Fe10 shows two broad maxima centered at ~0.15 and 0.25 nm *d* spacing. Such peak broadening generally result from the small particle size or the lack of long-range order. With increasing Cr content, the intensities of these two peaks gradually decrease; the XRD pattern of the Cr end member, Cr10, shows only a slight modulation of the background, indicating the lack of long-range periodicity in the structure and the likelihood of only short-range and possibly intermediate-range structure. The progressive diminution of the two broad maxima suggests progressive loss of the structure order and/or decrease in particle size along the compositional series.

3.3. X-ray Absorption Near-Edge Structure. We employed both Fe and Cr K-edge XANES spectroscopy, an element specific technique, to examine the differences in local coordination for each atom type as well as potential changes in oxidation state among samples.

We used Cr K-edge XANES spectroscopy to confirm the oxidation state and local symmetry of Cr in the compositional series. A pre-edge peak occurs in some Cr K-edge spectra because of the 1s to 3d electronic transition. This transition is dipole forbidden, but the probability of the transition increases as a result of Cr 3d and O 2p orbital mixing and the lack of a symmetry
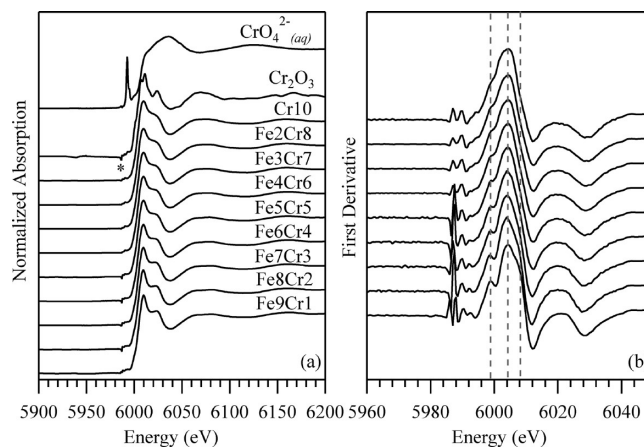
center. Consequently, spectra of Cr(VI) in tetrahedral coordination with oxygen exhibit a prominent pre-edge peak at ~5989 eV. In contrast, spectra for Cr(III)-containing compounds, with Cr having centrosymmetric octahedral coordination, exhibit a greatly reduced intensity for this pre-edge feature, with contributions mainly from quadrupolar transitions.[47,48] Oxidation state affects the position of the main edge, which is shifted to a higher energy for Cr(VI) relative to Cr(III). As shown in Figure 3a, a prominent pre-edge peak can be seen for CrO_4^{2-} (aq), whereas Cr_2O_3 exhibits no such feature and has a main edge position lower in energy. Via comparison of all our Cr_xFe_{1-x}-(oxy)hydroxide samples to the two reference compounds, it is clear that Cr(III) in octahedral coordination is the dominant species in the Cr_xFe_{1-x}-(oxy)hydroxide samples.

For Fe K-edge XANES, studies have shown that the energy position of the main absorption edge as well as the pre-edge peak in Fe XANES can be used for the determination of the Fe oxidation state (e.g., ref 49). Figure 4a shows the Fe K-edge XANES spectra of samples in the Cr_xFe_{1-x}-(oxy)hydroxide series as well as those for model compounds goethite and 2-line ferrihydrite. The main edge position of the whole sample series (at ~7130 eV) lines up well with that observed in goethite and 2-line ferrihydrite, suggesting Fe(III) as the dominant oxidation state in our sample series. In combination with the Cr XANES results, it is evident that no redox reactions have occurred in this system.

Figures 3b and 4b show the first derivatives of the Cr and Fe XANES, respectively. Clearly, the edge features show progressive changes along the sample series, including both intensity and position. These observations indicate

(47) Burns, R. G. *Mineralogical Application of Crystal Field Theory*, 2nd ed.; Cambridge University Press: New York, 1993.
(48) Brown, G. E.; Calas, G.; Waychunas, G. A.; Petiau, J. X-ray Absorption Spectroscopy: Applications in Mineralogy and Geochemistry. In *Reviews in Mineralogy*; Hawthorne, F. C., Ed.; Mineralogical Society of America: Chantilly, VA, 1988; Vol. *18*, pp 431−512.
(49) Prietzel, J.; Thieme, J.; Eusterhues, K.; Eichert, D. *Eur. J. Soil Sci.* **2007**, *58*(5), 1027–1041.
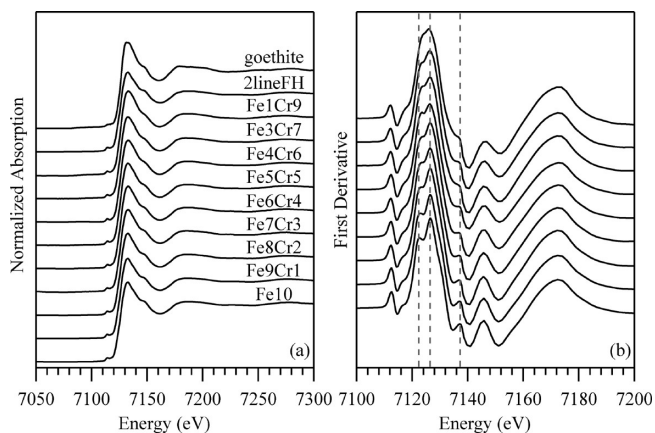
Figure 4. (a) Fe K-edge XANES spectra of Cr_xFe_{1-x}-(oxy)hydroxide samples and the model compounds goethite and 2-line ferrihydrite. (b) Corresponding first derivatives. Vertical dashed lines indicate the points at which progressive changes are observed.

progressive changes in the local structure around both the Cr and Fe atoms, consistent with chemical substitutions.

3.4. PDF Analysis. Reduced structure functions, $f(Q)$, and PDFs, $G(r)$, for all samples in the Cr_xFe_{1-x}-(oxy)hydroxide series and for the 2-line ferrihydrite model compound are shown in Figure 5, with increasing Cr content from bottom to top. Comparing the experimental structure functions, $f(Q)$, for the whole series, we find peaks are sharper and better resolved in samples with a higher Fe content (Figure 5a), whereas features become more broad and less distinct with an increasing Cr content.

The most striking trend observed in the PDFs for the Cr_xFe_{1-x}-(oxy)hydroxide series is a gradual and progressive decrease in the length scale of pair correlations with an increase in Cr content. The coherent scattering structural domain sizes of samples in the Cr_xFe_{1-x}-(oxy)hydroxide series are estimated from the attenuation of the real features in the PDFs and are listed in Table 1. Assuming no correlations greater than the longest interatomic distance in a single particle, no surface reconstruction, and a narrow particle size distribution, information about coherent domain size can, in certain cases, be used to determine average primary particle size.[50−52] Pair correlations in the PDF of Fe10 extend to 27 Å (full extent not shown in Figure 5b). In contrast, the oscillations corresponding to pair correlations in Cr10 are fully attenuated at ~10 Å. This loss of structure coherence beyond ~10 Å in Cr10 suggests that this phase is likely to have a much smaller average particle size and is exclusively short-range ordered, in contrast to the structural coherence extending over greater length scales in Fe10.

The reduced structure function and PDF for Fe10 are essentially identical to those for the 2-line ferrihydrite model compound (Figure 5), indicating that their atomic

arrangements are virtually identical. Slight differences observed in the amplitudes can be attributed to differences in the composition (e.g., amount of H_2O) used for normalization (Table 1). Ferrihydrite dried to different degrees has been shown to exhibit different amplitudes in PDF, which is due to differences in composition used for normalization and does not affect the essential structural information that is provided in the PDF (e.g., peak positions).[53] The Fe10 sample also seems to have a slightly greater coherent domain size than the 2-line ferrihydrite. Recent studies have shown great structural similarities among differently sized ferrihydrite forms.[53] On the basis of the structural similarities of Fe10 and ferrihydrite, and given that our experimental synthesis conditions are very similar to the standard synthesis methods for ferrihydrite,[36] it is likely that the Fe10 sample has a structure similar to that of ferrihydrite, with a coherent domain size of ~27 Å.

The sharpest peaks in the PDFs occur at low r values (1−4 Å) and contain information about the local coordination environments around Cr and Fe. Shown in an expanded view (Figure 6), the first prominent feature at ~2 Å corresponds to the metal−oxygen (M−O) pair correlation. Cr(III) and Fe(III) have similar ionic radii (0.615 and 0.645 Å, respectively)[54] and typical Cr(III)−O and Fe(III)−O distances of 1.96−1.98 Å in octahedral coordination. An idealized structure model was recently proposed for ferrihydrite,[55] containing ~20% tetrahedrally coordinated Fe(III) and ~80% octahedrally coordinated Fe(III) (Fe^{IV} and Fe^{VI}, respectively); large distortions in the first-neighbor oxygen coordination were reported along with overlap in the Fe^{IV}−O and Fe^{VI}−O distances. Although there has been recent debates concerning this model,[56−58] it nevertheless offers a useful framework for interpreting trends observed in the PDFs. Accordingly, the first peak in the PDF of Fe10 is expected to be dominated by the contributions of Fe^{VI}−O pairs with a smaller contribution from Fe^{IV}−O pairs. Averaging over these Fe−O distances associated with both coordination environments is probably the cause of the broadening of the first peak in Fe10 relative to samples with higher Cr contents. Cr(III) occurs almost exclusively in octahedral coordination with oxygen. The narrow peak at ~2 Å in Cr10 can therefore be understood to indicate a relatively narrow distribution of Cr−O distances, which is consistent with a single Cr coordination geometry. Correspondingly, the progressive trend toward a narrower peak width with an

(50) Hall, B. D.; Zanchet, D.; Ugarte, D. *J. Appl. Crystallogr.* **2000**, *33*, 1335–1341.
(51) Page, K.; Proffen, T.; Terrones, H.; Terrones, M.; Lee, L.; Yang, Y.; Stemmer, S.; Seshadri, R.; Cheetham, A. K. *Chem. Phys. Lett.* **2004**, *393*(4−6), 385–388.
(52) Egami, T.; Billinge, S. J. L. *Underneath the Bragg Peaks: Structural Analysis of Complex Materials*; Elsevier: Oxford, U.K., 2003; Vol. 7.

(53) Michel, F. M.; Ehm, L.; Liu, G.; Han, W. Q.; Antao, S. M.; Chupas, P. J.; Lee, P. L.; Knorr, K.; Eulert, H.; Kim, J.; Grey, C. P.; Celestian, A. J.; Gillow, J.; Schoonen, M. A. A.; Strongin, D. R.; Parise, J. B. *Chem. Mater.* **2007**, *19*(6), 1489–1496.
(54) Shannon, R. D. *Acta Crystallogr.* **1976**, *A32*, 751–767.
(55) Michel, F. M.; Ehm, L.; Antao, S. M.; Lee, P. L.; Chupas, P. J.; Liu, G.; Strongin, D. R.; Schoonen, M. A. A.; Phillips, B. L.; Parise, J. B. *Science* **2007**, *316*(5832), 1726–1729.
(56) Rancourt, D. G.; Meunier, J. F. *Am. Mineral.* **2008**, *93*(8−9), 1412–1417.
(57) Manceau, A. *Clay Miner.* **2009**, *44*(1), 19–34.
(58) Michel, F. M.; Barrón, V.; Torrent, J.; Morales, M. P.; Serna, C. J.; Boily, J. F.; Liu, Q. S.; Ambrosini, A.; Cismasu, A. C.; Brown, G. E. *Proc. Natl. Acad. Sci. U.S.A.* **2010**, *107*(7), 2787–2792.
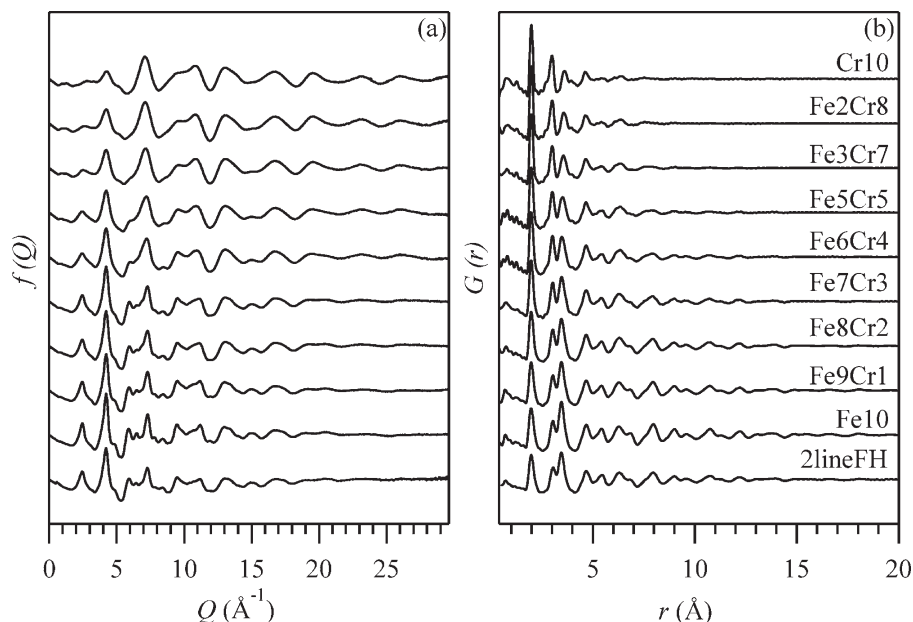
Figure 5. (a) Experimental reduced structure function $f(Q)$ and (b) corresponding calculated pair distribution function (PDF), also known as $G(r)$, for the Cr_xFe_{1-x}-(oxy)hydroxide sample series and 2-line ferrihydrite.
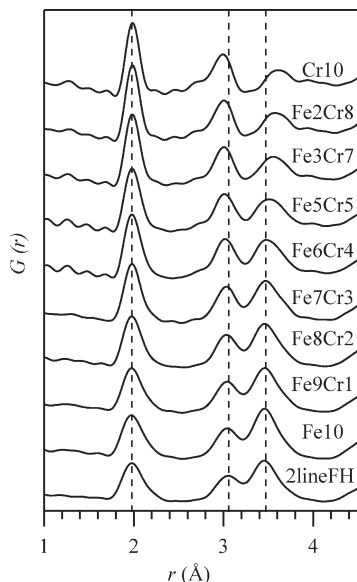

Figure 6. Expanded view of Figure 5b showing the PDFs of Cr_x-Fe_{1-x}-(oxy)hydroxide sample series and 2-line ferrihydrite with an r range of 1−4.5 Å.

increasing Cr content likely reflects a decreasing distribution of M−O distances as Cr(III) occupies octahedral sites.

The prominent pair correlations in Fe10 at ∼3.03 and 3.4 Å can be attributed dominantly to Fe−Fe correlations from highly distorted FeO_6 octahedra linked in edge-sharing and corner-sharing configurations, respectively. Smaller contributions are expected from O−O (∼2.8−3.0 Å) and Fe−O (∼3.5 Å) pair correlations,[55] which have weaker scattering relative to Fe−Fe pairs. With an increasing Cr content, the 3 Å peak shifts progressively to shorter distances with an additional peak at ∼2.7 Å appearing for Fe5Cr5, Fe3Cr7, Fe2Cr8, and Cr10, whereas the 3.4 Å peak shifts to longer distances and

decreases in intensity. It is more difficult to attribute these progressive shifts to changes in specific pair correlations, and we defer further interpretation pending development of a suitable structure model for the Cr10 sample.

3.5. HRTEM Analysis. HRTEM images and selected-area electron diffraction patterns (SAED) were obtained for the two end members and two intermediate composition samples: Fe10, Fe5Cr5, Fe3Cr7, and Cr10. Figure 7a shows the HRTEM image of Fe10. The average particle size is approximately 2−4 nm. The clear lattice fringes show that Fe10 is nanocrystalline or at least contains regions with ordering extending over nanometers. Sample Fe5Cr5 also shows clear lattice fringes. In contrast, lattice fringes are absent in HRTEM images of samples with a higher Cr content, i.e., Fe3Cr7 and Cr10 (Figure 7c,d). SAED patterns of Fe10, Fe5Cr5, and Fe3Cr7 (insets in Figure 7a−c) show two broad diffusion rings typical of materials lacking long-range order. These two rings have *d* spacings of ∼0.16 and 0.27 nm, consistent with the values from bulk XRD where two diffraction peaks at 0.15 and 0.25 nm are observed. The intensities of these two rings decrease with an increasing Cr content and eventually become indistinguishable for sample Cr10 (inset of Figure 7d), typical of an exclusively short-range ordered material. This is consistent with the bulk XRD observation where peak intensities decrease with an increasing Cr content. These observations are also consistent with PDF results where the length scale of structural order decreases with an increasing Cr content, from the intermediate-range order of Fe10 to the exclusively short-range order of Cr10. All four samples show strong aggregation.

4. Discussion

4.1. Physical Mixture versus Chemical Substitution. Two fundamental questions about the Cr_xFe_{1-x}-(oxy)hydroxide compositional series are whether the samples occur as
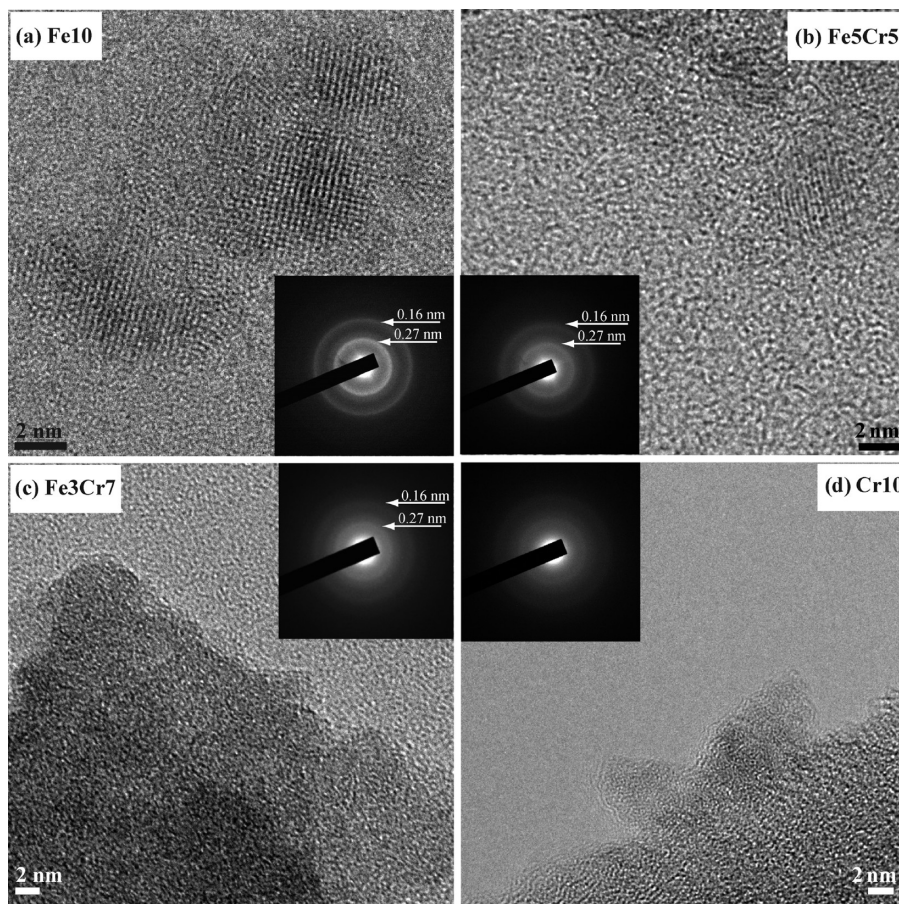
Figure 7. HRTEM images of (a) Fe10, (b) Fe5Cr5, (c) Fe3Cr7, and (d) Cr10 with selected-area electron diffraction patterns. Scale bars are 2 nm.

a physical mixture of two or more phases or are single-phase resulting from chemical substitution between Cr(III) and Fe(III), and whether that property changes along the series. Although XRD and PDF analyses do not yet provide full answers, complementary techniques such as XANES and TG-DSC analysis provide valuable constraints. XANES is an elemental specific technique that probes the local structure around a central atom. If the intermediate samples were physical mixtures of the end member, their Cr XANES should look exactly the same as that of the Cr10 end member because they share the same local coordination environment. Similarly, their Fe XANES should also be the same as that of the Fe10 end member. Therefore, the obseved gradual changes along the series provide strong evidence of Cr−Fe chemical substitution. Additional support for chemical substitution is found in the TG-DSC results. If sample Fe5Cr5 were a physical mixture of the end members, thermal signatures of each of the end members should be observed, which is not the case. Therefore, the thermal data argue against the intermediate sample being a physical mixture of the Cr and Fe end members.

4.2. Structural Changes along the Compositional Series. PDF and XANES analyses show a clear trend of progressive changes along the Cr_xFe_{1-x}-(oxy)hydroxide compositional series. However, understanding how such changes occur requires good structural models of both end members, as well as an understanding of the hydrolysis and precipitation processes involved in their forma-

tion. Observations from the X-ray total scattering data show clear differences between the Cr and Fe end members. The Fe end member has a structure similar to that of nanocrystalline ferrihydrite with a coherent domain size of ∼27 Å. In comparison, the Cr end member has a coherent domain size of ∼10 Å and lacks the intermediate-range order present in ferrihydrite.

Cr(III) and Fe(III) have very different ligand exchange behaviors in solution, resulting in different hydrolysis properties. The water exchange rate constant k_{ex} of the Cr(III) aqua ion $[Cr(OH_2)_6]^{3+}$ is 2.4×10^{-6} s^{-1}, much slower than that of the Fe(III) aqua ion $[Fe(OH_2)_6]^{3+}$ (160 s^{-1}).[59] The addition of base to Fe(III)-containing solutions causes rapid polymerization[22] and precipitation of insoluble (oxy)hydroxide (ferrihydrite), the structure of which has been extensively studied and widely considered as being nanocrystalline.[53,55,60]

Rapid alkalization of Cr(III)-containing solution leads to the immediate precipitation of a poorly crystalline "active chromium hydroxide" with the empirical formula $Cr(OH)_3 \cdot 3H_2O$, which can be effectively separated because of the kinetic inertness of the Cr(III) aqua ion.[20,22] Aging of this material in solution results in condensation and polymerization, leading to formation of an amorphous gel containing small oligomers, as reported

(59) Richens, D. T. *The Chemistry of Aqua Ions*; Wiley: Chichester, U.K., 1997.
(60) Jambor, J. L.; Dutrizac, J. E. *Chem. Rev.* **1998**, *98*(7), 2549–2585.

from both experiments and molecular dynamics simulations.[20,22,25] Such oligomerization is considered to be dependent on pH and solvent conditions and is slowest in the 6−7 pH range. A monomer was reported to be dominant (>91%) at pH ∼7 for aging up to 72 h.[20] Cr(III) pairs that link to neighbors via two μ-OH bridges were also reported to be important, which likely accounts for the structure of small oligomers, such as dimers and ring trimers.[25] Such differences in ligand exchange rates between Cr and Fe might also account for the observation of the longer-range order in the Fe end member, i.e., greater crystallinity, compared to that of the Cr end member.

With this information, we are unable to deduce a structure model for our Cr end member. Given our experimental conditions and the small coherent domain size observed for Cr10 (∼10 Å), it is likely to consist of small oligomer(s).

Despite clear differences in the structural properties of Cr10 and Fe10, they share some similarities, including a lack of long-range order and the presence of edge sharing of metal octahedra, as demonstrated by M−M distances of ∼3 Å observed for both samples. These similarities might serve as the basis for the progressive structural changes observed along the compositional series. However, since we do not have a structure model for the Cr end member, it is not clear how such structural changes occur.

4.3. Solid Solution? The traditional definition of a solid solution embraced by many researchers requires the end members to have the same structure, with isomorphic substitution on one or more sites.[61] However, the differences in structural properties that we observe between the Cr and Fe end members suggest that the associated compositional series should not be considered a traditional solid solution. Nevertheless, the progressive changes observed in PDF and XAS data along the compositional series pose interesting questions such as how continuous chemical substitutions are accommodated between two structurally different compounds or whether there are constraints that cannot be reconciled by continuous substitution. The Fe end member, ferrihydrite, has recently been proposed to contain octahedrally and tetrahedrally coordinated Fe(III).[55] It is known that Cr(III) occurs almost exclusively in octahedral coordination. Therefore, Cr(III) substitution along the compositional series would presumably be limited to octahedral sites and not random. Further investigations are needed to determine the structure of the Cr end member and to provide a more detailed understanding of the structural changes along the compositional series. On the other hand, it is also widely accepted that materials with nanoscale size commonly exhibit different structural properties compared to those of their bulk counterpart, e.g., large surface distortion. This suggests that the traditional definition of a solid solution needs to be reexamined at the nanoscale.

5. Conclusions

In this study, we employed complementary techniques to examine the structural properties of Cr_xFe_{1-x}-(oxy)-hydroxides. Our bulk X-ray diffraction data show that the Cr_xFe_{1-x}-(oxy)hydroxide sample series has poorly resolved and/or broad diffraction features, due to the lack of long-range order and/or the effects of small particle size. Thermal analysis indicates that Cr10 has a higher water content than Fe10 and shows three stages of weight loss due to the dehydration of surface-adsorbed water, followed by the loss of structural water and an exothermic transition process. The intermediate sample Fe5Cr5 exhibits a loss of structural water at a lower temperature than the Cr end member Cr10, whereas its temperature for the exothermic transition is higher. PDF results suggest that Cr10 and Fe10 have different structures and different coherent domain sizes. Cr10 exhibits only short-range order, with a coherent domain size of ∼10 Å, consistent with the high surface water content. Fe10 has a coherent domain size of ∼27 Å and a structure similar to that of nanocrystalline 2-line ferrihydrite. XANES analysis shows Cr(III) and Fe(III) to be the dominant oxidation states in our samples, indicating no redox reactions in the system. PDF shows progressive structural changes across the series, and XANES spectra also show progressive changes in the local structure around Cr and Fe atoms. These observations provide strong structural evidence of chemical substitutions and progressive structural changes along the whole compositional series. Given that Cr(III) predominantly exists in octahedral coordination, substitution of Cr into the Fe end member, ferrihydrite, might be limited to octahedral sites.

Note Added after ASAP Publication. There was a minor text error in Table 1 in the version published ASAP May 18, 2010; the corrected version was published ASAP May 20, 2010.

(61) Shriver, D. F.; Atkins, P.; Langford, C. H. *Inorganic Chemistry*, 2nd ed.; W. H. Freeman and Co.: New York, 1994.

Supporting Information Available: Description of the preparation, PDF data collection, and analysis of the physical mixtures of Cr10 and Fe10, principal component analysis and linear combination fits on the PDFs of physical mixtures, a table of the sample information and linear combination fit results of the physical mixtures, a table of the Fe:Cr molar ratio of samples Fe5Cr5 and Fe3Cr7 from energy dispersive spectra analysis, a figure of the original and reconstructed $G(r)$ of the mixtures using the two primary components determined from principal component analysis, a figure of the linear combination fits of $G(r)$ of the mixture sample series using Fe10 and Cr10 as end members, and a figure of representative energy dispersive spectra of samples Fe10, Fe5Cr5, Fe3Cr7, and Cr10. This material is available free of charge via the Internet at http://pubs.acs.org.